

Incorporating sparse labels into hidden Markov models using weighted likelihoods improves accuracy and interpretability in biologging studies

Evan Sidrow^{1*}, Nancy Heckman¹, Tess M. McRae², Beth L. Volpov², Andrew W. Trites^{2,3}, Sarah M. E. Fortune^{2,4}, Marie Auger-Méthé^{1,2}

1 Department of Statistics, University of British Columbia, Vancouver, BC, Canada

2 Institute for the Oceans and Fisheries, University of British Columbia, Vancouver, BC, Canada

3 Department of Zoology, University of British Columbia, Vancouver, BC, Canada

4 Department of Oceanography, Dalhousie University, Halifax, NS, Canada

* evan.sidrow@stat.ubc.ca

Key words and phrases: Biologging; killer whales; mixture models; semi-supervised learning; statistical ecology; time series.

Abstract

Ecologists often use a hidden Markov model to decode a latent process, such as a sequence of an animal’s behaviours, from an observed biologging time series. Modern technological devices such as video recorders and drones now allow researchers to directly observe an animal’s behaviour. Using these observations as labels of the latent process can improve a hidden Markov model’s accuracy when decoding the latent process. However, many wild animals are observed infrequently. Including such rare labels often has a negligible influence on parameter estimates, which in turn does not meaningfully improve the accuracy of the decoded latent process. We introduce a weighted likelihood approach that increases the relative influence of labelled observations. We use this approach to develop two hidden Markov models to decode the foraging behaviour of killer whales (*Orcinus orca*) off the coast of British Columbia, Canada. Using cross-validated evaluation metrics, we show that our weighted likelihood approach produces more accurate and understandable decoded latent processes compared to existing methods. Thus, our method effectively leverages sparse labels to enhance researchers’ ability to accurately decode hidden processes across various fields.

1 Introduction

The hidden Markov model, or HMM, is a common statistical model that is increasingly being used to understand the movements and behaviours of animals [22, 29, 41]. An HMM is a generalization of a mixture model that is used to decode a latent process of interest (e.g., a sequence of animal behaviours) from an observed time series (e.g., biologging data from tags attached to the animal). They have been used to uncover a wide variety of animal behaviours, including foraging activity [20, 51] and habitat selection [17].

Many ecological studies employ *unsupervised* HMMs, meaning that the true behaviours of the study animals are never directly observed and instead are predicted entirely from biologging data [1, 19, 30, 31]. However, ecologists are often interested in predicting complicated animal behaviours (e.g., successful prey captures) that are difficult to identify from movement data alone [43]. For these behaviours, the relationship between an animal’s behaviour and its movement is so complex that it is rarely fully characterized by a statistical model.

One solution to better characterize what animals are doing is to fully observe and incorporate the animal’s behaviours into the underlying model, in which case the HMM is *fully supervised*. Krogh et al. [18] showed that fully supervised HMMs exhibit better predictive performance than unsupervised HMMs in various settings, and fully supervised HMMs are used in fields ranging from speech recognition to medicine [3, 42]. To our knowledge fully supervised HMMs are rare in ecology, but some animal behaviour studies use other fully supervised machine learning techniques [2, 6]. However, these studies often focus on captive animals that are much easier to continuously observe compared to wild animals.

While fully observing an animal’s behaviour in the wild can be prohibitively difficult or expensive, many ecological studies have behavioural information for a small subset of time. Occasional observations of an animal’s behaviour can be incorporated into a *semi-supervised* HMM, and some notable ecological studies have used semi-supervised HMMs. For example, McClintock et al. [21] labelled a subset of hidden behavioural states of a grey seal (*Halichoerus grypus*) using its proximity to known “haul-out” and foraging sites. Alternatively, Pirotta et al. [31] assumed that northern fulmars (*Fulmarus glacialis*) begin every journey in some known behavioural state. Other studies that used semi-supervised HMMs include McRae et al. [25], who used drone footage to directly label the behaviour of killer whales (*Orcinus orca*) for a subset of observation times, and Saldanha et al. [35], who used a multi-sensor approach to derive behavioural labels for red-billed tropicbirds (*Phaethon aethereus*). All of these studies demonstrate that incorporating partial labels into an ecological HMM can significantly improve its performance.

While behavioural labels can improve an HMM’s prediction accuracy, many ecological studies only have access to labels for a small proportion of observations (e.g., < 10%) [25, 35]. In these cases, the labelled data often do not meaningfully affect the parameter estimates of an HMM because the likelihood is dominated by the unlabelled data [7, 34]. A study by Ji et al. [15] used a weighted likelihood approach to increase the influence of labelled examples, but it assumed that labels correspond to independent time series. This approach does not apply when labels occur *within* a time series, which is often the case for ecological studies [25, 35].

Foraging behaviour can be especially rare and difficult to identify, but it is often of prime interest in ecology [35, 40]. For example, understanding foraging behaviour is vital for the conservation of northern and southern resident killer whales off the coast of British Columbia [16, 20, 45]. Although both sub-populations have dietary and spatial overlap, northern residents (threatened) have a positive growth trajectory compared to southern residents (endangered) [8, 45]. Studies have shown that various factors contribute to these population trends, including prey availability, anthropogenic pollutants, and vessel disturbances, but the exact causal mechanisms are not fully understood [16, 20, 26]. Each of these factors affects foraging ecology differently, so understanding how often and how successfully these sub-populations hunt may help explain differences in their population trajectories [28, 45].

We introduce a novel weighted semi-supervised learning approach for hidden Markov models that allows practitioners to adjust the influence of sparse labels within a time series. We first review the definition of an HMM and current semi-supervised learning techniques for mixture models that lack time dependence. We then formalize a *partially hidden Markov model*, or PHMM, which is designed to account for time series that are partially labelled, before introducing a weighted likelihood approach to balance the influence of labelled and unlabelled data within the model. Finally, we present two case studies that use labels derived from video data and our weighted likelihood approach to achieve higher cross-validated accuracy compared to existing baseline methods.

2 Background

Hidden Markov models

Hidden Markov models describe time series that exhibit state-switching behaviour. They model an observed time series of length T , $\mathbf{Y} = \{Y_t\}_{t=1}^T$, by assuming that each observation Y_t is generated from an unobserved hidden state $X_t \in \{1, \dots, N\}$. The sequence of all hidden states $\mathbf{X} = \{X_t\}_{t=1}^T$

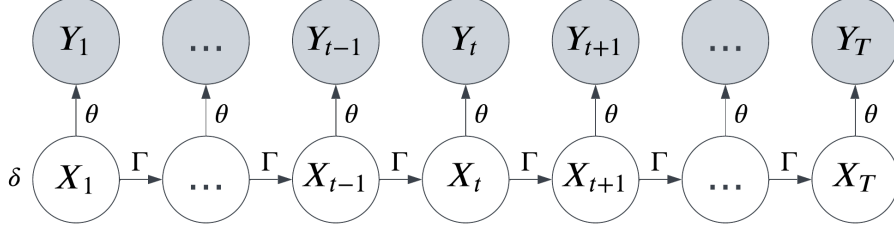


Fig 1. Graphical representation of an HMM. X_t corresponds to an unobserved latent state at time t whose distribution is described by a Markov chain. Y_t corresponds to an observation at time t , where Y_t given all other observations $\mathbf{Y} \setminus \{Y_t\}$ and hidden states \mathbf{X} depends only on X_t .

is modelled as a Markov chain. The unconditional distribution of X_1 is denoted by the row-vector $\boldsymbol{\delta} = (\delta^{(1)} \dots \delta^{(N)})$, where $\delta^{(i)} = \mathbb{P}(X_1 = i)$. Further, the distribution of X_t given X_{t-1} for $t = 2, \dots, T$ is denoted by the N -by- N transition probability matrix

$$\mathbf{\Gamma}_t = \begin{pmatrix} \Gamma_t^{(1,1)} & \dots & \Gamma_t^{(1,N)} \\ \vdots & \ddots & \vdots \\ \Gamma_t^{(N,1)} & \dots & \Gamma_t^{(N,N)} \end{pmatrix}, \quad (1)$$

where $\Gamma_t^{(i,j)} = \mathbb{P}(X_t = j \mid X_{t-1} = i)$. For simplicity, we assume that $\mathbf{\Gamma}_t$ does not change over time (i.e. $\mathbf{\Gamma}_t = \mathbf{\Gamma}$ for all t) unless stated otherwise.

Each observation Y_t is a random variable, where Y_t given all other observations ($\mathbf{Y} \setminus \{Y_t\}$) and hidden states (\mathbf{X}) depends only on X_t . If $X_t = i$, then the conditional density or probability mass function of Y_t is $f^{(i)}(\cdot; \theta^{(i)})$, where $\theta^{(i)}$ are the parameters describing the state-dependent distribution of Y_t . The collection of all state-dependent parameters is $\boldsymbol{\theta} = \{\theta^{(i)}\}_{i=1}^N$. A fixed realization of \mathbf{Y} is denoted as $\mathbf{y} = \{y_t\}_{t=1}^T$ and has probability density function

$$p(\mathbf{y} ; \boldsymbol{\delta}, \mathbf{\Gamma}, \boldsymbol{\theta}) = \boldsymbol{\delta} P(y_1; \boldsymbol{\theta}) \prod_{t=2}^T \mathbf{\Gamma} P(y_t; \boldsymbol{\theta}) \mathbf{1}_N^\top, \quad (2)$$

where $\mathbf{1}_N$ is an N -dimensional row vector of ones and $P(y_t; \boldsymbol{\theta})$ is an $N \times N$ diagonal matrix with entry (i, i) equal to $f^{(i)}(y_t; \theta^{(i)})$. Parameter estimation for HMMs often involves maximizing Eq (2) with respect to $\boldsymbol{\delta}$, $\mathbf{\Gamma}$, and $\boldsymbol{\theta}$. Fig 1 shows an HMM as a graphical model. For a more complete introduction to HMMs, see Zucchini et al. [52].

Semi-supervised mixture models

Semi-supervised learning is a paradigm in machine learning that harnesses both labelled and unlabelled data to enhance model performance [7]. There is a large taxonomy of semi-supervised learning techniques, but here we focus on generative mixture models because an HMM is a generalization of a mixture model that includes serial dependence between its hidden states [27, 46]. Unfortunately, many semi-supervised learning techniques for mixture models do not account for the time dependence of HMMs. As such, we build off of current approaches for mixture models and develop a novel semi-supervised learning technique for HMMs.

A mixture model is a simpler version of a hidden Markov model where the hidden states $\mathbf{X} = \{X_t\}_{t=1}^T$ are modelled as independent categorical random variables instead of a Markov chain. The distribution of X_t is denoted by the row-vector $\boldsymbol{\pi} = (\pi^{(1)} \dots \pi^{(N)})$ for all $t = 1, \dots, N$, where $\pi^{(i)} = \mathbb{P}(X_t = i)$. A sequence of observations $\mathbf{y} = \{y_t\}_{t=1}^T$ then has the probability density function

$$p(\mathbf{y} ; \boldsymbol{\pi}, \boldsymbol{\theta}) = \prod_{t=1}^T \left(\sum_{i=1}^N \pi^{(i)} f^{(i)}(y_t; \theta^{(i)}) \right). \quad (3)$$

Now, suppose that a subset of time indices $\mathcal{T} \subseteq \{1, \dots, T\}$ have corresponding labels $\mathbf{Z} = \{Z_t\}_{t \in \mathcal{T}}$. Labels are often observed at random times (e.g., aerial drones observe whale behaviours at random times), but we assume that \mathcal{T} is fixed, as is common for many semi-supervised learning techniques [7, 14]. Like Y_t , each label Z_t is a random variable generated from its corresponding hidden state X_t . The state space of Z_t is general, but for simplicity we assume that $Z_t \in \{1, \dots, N\}$. Given all other labels ($\mathbf{Z} \setminus \{Z_t\}$), observations (\mathbf{Y}), and hidden states (\mathbf{X}), we assume that Z_t depends only on X_t for each $t \in \mathcal{T}$. If $X_t = i$, then the label Z_t has probability mass function $g^{(i)}(\cdot; \beta^{(i)})$, with parameters $\beta^{(i)}$. Denote a fixed realization of labels \mathbf{Z} as $\mathbf{z} = \{z_t\}_{t \in \mathcal{T}}$. Then, the joint probability density of \mathbf{y} and \mathbf{z} for semi-supervised mixture models is

$$p(\mathbf{y}, \mathbf{z}; \boldsymbol{\pi}, \boldsymbol{\theta}, \boldsymbol{\beta}) = \prod_{t \in \mathcal{T}} \left(\sum_{i=1}^N \pi^{(i)} f^{(i)}(y_t; \theta^{(i)}) g^{(i)}(z_t; \beta^{(i)}) \right) \prod_{t \notin \mathcal{T}} \left(\sum_{i=1}^N \pi^{(i)} f^{(i)}(y_t; \theta^{(i)}) \right), \quad (4)$$

where $\boldsymbol{\beta} = \{\beta^{(i)}\}_{i=1}^N$. To write Eq (4) in a simpler form, we define $z_t = \emptyset$ for all unlabelled observations (i.e., for all $t \notin \mathcal{T}$) and set $g^{(i)}(\emptyset; \beta^{(i)}) = 1$. This abuse of notation results in a relatively simple probability density function for semi-supervised mixture models:

$$p(\mathbf{y}, \mathbf{z}; \boldsymbol{\pi}, \boldsymbol{\theta}, \boldsymbol{\beta}) = \prod_{t=1}^T \left(\sum_{i=1}^N \pi^{(i)} f^{(i)}(y_t; \theta^{(i)}) g^{(i)}(z_t; \beta^{(i)}) \right). \quad (5)$$

Eq (5) can be used to construct a likelihood and maximized with respect to $\boldsymbol{\pi}$, $\boldsymbol{\theta}$, and $\boldsymbol{\beta}$ to perform semi-supervised inference on mixture models [7]. In some scenarios, subject matter experts can identify the labels \mathbf{z} with certainty. In this case, $Z_t = X_t$ for all $t \in \mathcal{T}$, the parameters $\boldsymbol{\beta}$ do not need to be inferred, and $g^{(i)}$ takes the form

$$g^{(i)}(z_t) = \begin{cases} 1, & z_t \in \{i, \emptyset\}, \\ 0, & z_t \notin \{i, \emptyset\}. \end{cases} \quad (6)$$

We define $g^{(i)}$ as in Eq (6) for the case studies. However, if subject matter experts are not confident in their labels, we recommend parameterizing $g^{(i)}$ and inferring the parameters $\boldsymbol{\beta}$.

Weighted likelihood for semi-supervised mixture models

One issue in semi-supervised learning occurs when the number of observations T is much larger than the number of labels $|\mathcal{T}|$. In this case, the labelled data do not meaningfully affect maximum likelihood parameter estimates [7]. As a solution, Chapelle et al. [7] introduce a parameter $\lambda \in [0, 1]$ which represents the relative weight given to unlabelled observations. In particular, they define a weighted likelihood $\tilde{\mathcal{L}}_\lambda$ based on Eq (5) with weights \tilde{w}_λ as follows:

$$\tilde{w}_\lambda(z_t) = \begin{cases} (1 - \lambda) \frac{T}{|\mathcal{T}|}, & z_t \in \{1, \dots, N\} \\ \lambda \frac{T}{T - |\mathcal{T}|}, & z_t = \emptyset \end{cases}, \quad (7)$$

$$\tilde{\mathcal{L}}_\lambda(\boldsymbol{\pi}, \boldsymbol{\theta}, \boldsymbol{\beta}; \mathbf{y}, \mathbf{z}) = \prod_{t=1}^T \left(\sum_{i=1}^N \pi^{(i)} f^{(i)}(y_t; \theta^{(i)}) g^{(i)}(z_t; \beta^{(i)}) \right)^{\tilde{w}_\lambda(z_t)}. \quad (8)$$

Using this formulation, setting $\lambda = 0$ throws out all unlabelled data, setting $\lambda = 1$ throws out all labelled data, and setting $\lambda = (T - |\mathcal{T}|)/T$ returns a likelihood that corresponds to the joint density from Eq (5). It is unlikely that a practitioner would prefer setting $\lambda > (T - |\mathcal{T}|)/T$, as this weights unlabelled observations more heavily than labelled observations. In practice, researchers often select λ by performing cross-validation with an appropriate model evaluation metric [7].

The weighted likelihood $\tilde{\mathcal{L}}_\lambda$ is a specific instance of a much more general class of relevance-weighted likelihoods that has been studied extensively. Hu et al. [14] provide a comprehensive

review of weighted likelihoods. Applying their paradigm to this research, the probability density of the labelled data $\{Y_t, Z_t\}_{t \in \mathcal{T}}$ is given by Eq (4), but the probability density of the unlabelled data $\{Y_t\}_{t \notin \mathcal{T}}$ is some unknown density that “resembles” the density of the labelled data in some sense. In particular, Hu et al. [14] formally define the notion of “resemblance” using Boltzman’s entropy, and the weight λ corresponds to how much the density of the unlabelled data resembles the density of the labelled data under this definition. Hu et al. [12] prove the consistency and asymptotic normality of maximum weighted likelihood estimators under certain regularity conditions. The relevance-weighted likelihood literature thus gives useful theoretical guarantees related to the weighted likelihood for mixture models. Unfortunately, these guarantees usually assume that the observations \mathbf{y} are independent, which is not true for HMMs.

3 Weighted likelihood for semi-supervised learning in hidden Markov models

Our weighted likelihood approach for semi-supervised learning in HMMs begins by writing down the probability density associated with a partially observed HMM. We use the same notation as described above, namely random labels $\mathbf{Z} = \{Z_t\}_{t \in \mathcal{T}}$, where Z_t is generated from hidden state X_t and, conditioned on \mathbf{X} , \mathbf{Y} , and $\mathbf{Z} \setminus \{Z_t\}$, Z_t depends only on X_t . As before, a fixed realization of \mathbf{Z} is denoted as $\mathbf{z} = \{z_t\}_{t \in \mathcal{T}}$, and we abuse notation by setting $z_t = \emptyset$ for all unlabelled observations (i.e., $t \notin \mathcal{T}$) and $g^{(i)}(\emptyset; \beta^{(i)}) = 1$. The joint density of the observations \mathbf{y} and labels \mathbf{z} for an HMM is thus

$$p(\mathbf{y}, \mathbf{z}; \boldsymbol{\delta}, \boldsymbol{\Gamma}, \boldsymbol{\theta}, \boldsymbol{\beta}) = \delta P(y_1, z_1; \boldsymbol{\theta}, \boldsymbol{\beta}) \prod_{t=2}^T \boldsymbol{\Gamma} P(y_t, z_t; \boldsymbol{\theta}, \boldsymbol{\beta}) \mathbf{1}_N^\top, \quad (9)$$

where $P_t(y_t, z_t; \boldsymbol{\theta}, \boldsymbol{\beta})$ is an $N \times N$ diagonal matrix where entry (i, i) is $f^{(i)}(y_t; \theta^{(i)})g^{(i)}(z_t; \beta^{(i)})$. We refer to this model as a *partially hidden Markov model*, or PHMM.

Incorporating partial labels in an HMM to define a PHMM is relatively straightforward, but defining a weighted likelihood for PHMMs is more complicated. Recall that each term in Eq (8) is a scalar value raised to the power of some weight. However, each term in Eq (9) is a matrix, so it is not straightforward to raise each term to the power of a (possibly fractional) weight. While it is possible to calculate fractional powers of matrices, doing so can be computationally expensive and the result can be difficult to interpret [11]. Alternatively, Hu et al. [13] derive a relevance-weighted likelihood for dependent data using the same paradigm as Hu et al. [14]. Although their method is broadly applicable, it does not apply to HMMs. Namely, they adopt a paradigm where each observation Y_t has a corresponding set of parameters $\{\boldsymbol{\delta}_t, \boldsymbol{\Gamma}_t, \boldsymbol{\theta}_t\}$, and they assume that Y_t depends only on its corresponding parameters and the previous observations $\{Y_s\}_{s=1}^{t-1}$. However, this assumption is violated for an HMM because Y_t depends on X_t , which in turn depends upon the previous parameters $\{\boldsymbol{\delta}_s, \boldsymbol{\Gamma}_s, \boldsymbol{\theta}_s\}_{s=1}^{t-1}$. See Eq (3) of Hu et al. [13] for more details.

A weighted likelihood for PHMMs should have three desired properties. First, the weighted likelihood should reduce to Eq (9) for some “natural” weight, just as $\lambda = (T - |\mathcal{T}|)/T$ does for the weighted likelihood in Eq (8). Second, some weight should correspond to ignoring all unlabelled data, just as $\lambda = 0$ does for the weighted likelihood in Eq (8). These two properties allow practitioners to intuitively select a weight that balances a natural weighting scheme with one that completely ignores all unlabelled data. Finally, the weighted likelihood should be relatively simple and intuitive compared to the standard likelihood from Eq (9). We thus propose the weighting parameter $\alpha \in [0, 1]$ and the following weighted likelihood for partially hidden Markov models:

$$w_\alpha(z_t) = \begin{cases} 1, & z_t \in \{1, \dots, N\} \\ \alpha, & z_t = \emptyset \end{cases}, \quad (10)$$

$$\mathcal{L}_\alpha(\boldsymbol{\delta}, \boldsymbol{\Gamma}, \boldsymbol{\theta}, \boldsymbol{\beta}; \mathbf{y}, \mathbf{z}) = \delta P(y_1, z_1; \boldsymbol{\theta}, \boldsymbol{\beta})^{w_\alpha(z_1)} \prod_{t=2}^T \boldsymbol{\Gamma} P(y_t, z_t; \boldsymbol{\theta}, \boldsymbol{\beta})^{w_\alpha(z_t)} \mathbf{1}_N^\top, \quad (11)$$

This formulation satisfies the three desired properties listed above. First, if $\alpha = 0$, then the term corresponding to an unlabelled observation t is $\Gamma P(y_t, z_t; \boldsymbol{\theta}, \boldsymbol{\beta})^0 = \Gamma$. Therefore, the likelihood of a PHMM with $\alpha = 0$ is identical to the likelihood of an HMM that treats all unlabelled observations as totally missing [52]. Next, if $\alpha = 1$, then the term corresponding to an unlabelled observation t is $\Gamma P(y_t, z_t; \boldsymbol{\theta}, \boldsymbol{\beta})^1 = \Gamma P(y_t, z_t; \boldsymbol{\theta}, \boldsymbol{\beta})$. In this case, the weighted PHMM likelihood in Eq (11) corresponds to the standard PHMM density in Eq (9). Finally, we argue that this formulation is intuitive, as it weights unlabelled observations using some power of α and leaves labelled observations unaltered. Fig 2 shows graphical representations of PHMMs for several values of α with only Z_1 , Z_{t-1} , and Z_{t+1} observed for some fixed t .

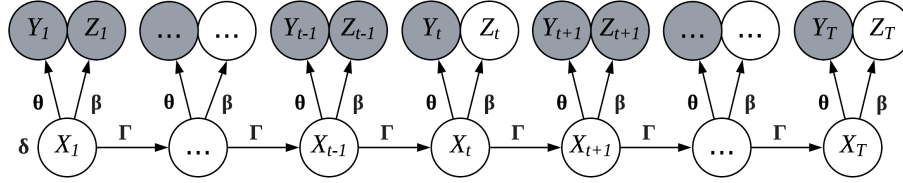
We recommend that practitioners use the following cross-validation procedure to find an optimal value of α . First, select a range of candidate values of $\alpha \in [0, 1]$. We recommend testing at least $\alpha \in \{0, |\mathcal{T}|/(T - |\mathcal{T}|), 1\}$, as $\alpha = |\mathcal{T}|/(T - |\mathcal{T}|)$ approximately balances the influence of labelled and unlabelled observations in the likelihood. While it is technically possible, we do not recommend considering $\alpha > 1$ because doing so weights unlabelled observations more heavily than labelled observations. Second, divide the time series data set into several “folds” for cross validation. Third, train the PHMM on the full data set while ignoring a fold, and use the forward-backward algorithm on the held-out fold (ignoring its associated labels) to estimate the hidden state probabilities $\mathbb{P}(X_t | \mathbf{Y} = \mathbf{y})$. Fourth, repeat the previous step for all folds to estimate the cross-validated hidden state probabilities for the entire data set. Finally, use the estimated probabilities and true labels together with standard model validation techniques to evaluate the resulting PHMM and select the most appropriate value of α . This cross-validation procedure can be computationally expensive, especially for large datasets. Practitioners can train PHMMs on all folds in parallel to reduce computation time, and we used the Cedar Compute Canada cluster to perform cross-validation in parallel for the case studies.

4 Case studies

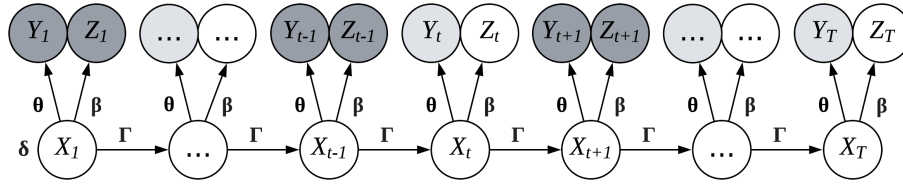
We conducted two case studies that use PHMMs to model the behaviour and foraging success of 11 resident killer whales (nine northern, two southern) off the coast of British Columbia, Canada. These case studies were primarily intended to test the predictive performance of the PHMM and demonstrate the process of applying it to ecological data. However, we also performed these case studies for their ecological significance. As mentioned earlier, understanding killer whale foraging and successful prey capture has been a research focus for years, as differences in foraging success may explain why the southern resident killer whale population is doing poorly compared to the northern residents [28, 45]. Thus, the results from these case studies can help ecologists correctly predict foraging behaviours that are meaningful for conservation.

The data for these case studies were collected in August and September 2020 using a time-depth recorder (TDR) tag from Customizable Animal Tracking Solutions (www.cats.is). All resident killer whales were tagged with suction-cup attached tags as described by McRae et al. [25]. These tags were deployed using an adjustable 6-8 meter carbon fiber pole and detached using galvanic releases. Post-deployment, the instruments were retrieved utilizing a combination of a Wildlife Computers 363C SPOT tag (providing Argos satellite positions), a goniometer, an ultra high frequency receiver, and a yagi antenna. The tags were equipped with an array of instruments, including 3D kinematic sensors (accelerometer, magnetometer, gyroscope), a time-depth recorder, a 96kHz HTI hydrophone, and a camera. The TDR and inertial sensors were set to sample at a frequency of 50 Hz. Depth readings were calibrated using a MATLAB package developed by Cade et al. [5], which allowed for the extraction of heading, pitch, and roll, as well as three-dimensional dynamic acceleration within the reference frame of the killer whale.

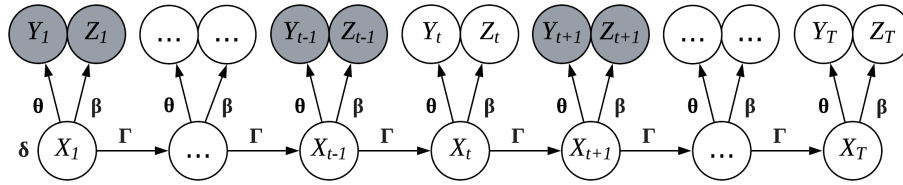
Using these data, we developed two PHMMs to identify killer whale foraging behaviours at different scales. The first PHMM estimated killer whale dive types using individual dives as observations, with some dives labelled as resting, travelling, or foraging using drone videos. The second PHMM estimated prey capture events using high-frequency biologging data as observations, with



(a) Partially hidden Markov model with $\alpha = 1$. This PHMM gives equal weight to all observations in the likelihood function. This is the “natural” formulation of a PHMM with missing labels.



(b) Partially hidden Markov model with $\alpha \in (0, 1)$. This PHMM weights the influence of Y_t, Y_T , and all other observations that do not have associated observed labels. However, it does not ignore them altogether.



(c) Partially hidden Markov model with $\alpha = 0$. This PHMM ignores all observations that do not have associated label information. In particular, Y_t, Y_T , and all other observations that do not have observed labels are treated as unobserved.

Fig 2. Graphical representation of various PHMMs with likelihood weightings (a) $\alpha = 1$, (b) $\alpha \in (0, 1)$ and (c) $\alpha = 0$. The colour (white, light grey, and dark grey) indicates how much a given observation affects the weighted likelihood. White corresponds to treating the random variable as unobserved, dark grey corresponds to treating the variable as fully observed, and light grey corresponds to treating the random variable as observed, but weighting it in the likelihood. The latent states are denoted as $\{X_{t'}\}_{t'=1}^T$, the observations are denoted as $\{Y_{t'}\}_{t'=1}^T$, and labels are denoted as $\{Z_{t'}\}_{t'=1}^T$. In this example, Z_1, Z_{t-1} , and Z_{t+1} are observed, while all other labels are unobserved (i.e., $Z_{t'} = \emptyset$ for $t' \neq 1, t-1, t+1$).

some observations labelled using underwater video and audio recordings of prey capture. For both case studies, we modelled each killer whale as independent, but with shared parameters for their associated PHMMs.

Labels were identified with high confidence in both case studies, so we defined $g^{(i)}$ according to Eq (6). We also used k -fold cross-validation to calculate evaluation metrics in both case studies. In particular, we divided the data from all killer whales into k folds, removed a fold from the original dataset, and fit the model using 10 random parameter initialization and a custom version of the momentuHMM package in R [23, 33]. We then used the forward-backward algorithm on the held-out fold (while ignoring its true labels) to obtain estimated probabilities of each hidden state (dive phase or dive type). We repeated this process for each fold to obtain hidden state probability estimates for the entire data set.

Case study 1: behavioural classification of killer whale dives

For our first case study, we assigned a latent behaviour to every killer whale dive. To this end, we modelled the data from each killer whale as a sequence of dives and modelled each sequence with a PHMM. The hidden Markov chain was a sequence of dive types and the observations were summary statistics of each dive. We used three well-known killer whale behaviours as possible dive types: resting, travelling, and foraging [24, 50]. We also used aerial and underwater recordings to label a small subset of dives with one of these dive types (see Table 2 McRae et al. [25]).

Data processing

We defined a dive as any period in which the killer whale was below a depth of 0.5 meters for at least 30 seconds, which includes only biologically meaningful dives and excludes surface behaviours. In line with previous studies [19, 25], we summarized each dive with its maximum depth and total duration. Formally, the observation associated with whale s and dive t was denoted as $y_{s,t} = (m_{s,t}, d_{s,t})$, where $m_{s,t}$ corresponds to maximum depth in meters and $d_{s,t}$ corresponds to dive duration in seconds. This process resulted in time series for $S = 11$ killer whales, who together performed a total of $T = 2169$ dives.

Using drone videos, we visually identified three diving behaviours: resting, travelling, and foraging (classification criteria are given in Table 2 of McRae et al. [25]). Formally, the label associated with whale s and dive t was denoted as $z_{s,t} \in \{\emptyset, 1, 2, 3\}$, where each value of $z_{s,t}$ corresponds to either no label (if $z_{s,t} = \emptyset$), resting (if $z_{s,t} = 1$), travelling (if $z_{s,t} = 2$), or foraging (if $z_{s,t} = 3$). This resulted in a total of $|\mathcal{T}| = 106$ labels for dive types.

Model formulation

We used a PHMM with $N = 3$ dive types to match the drone-identified labels of resting, travelling, and foraging dives. For whale s and dive t , we denoted the hidden dive type as $X_{s,t} \in \{1, 2, 3\}$. Histograms and scatter plots revealed that dive duration and maximum depth looked to be distributed approximately as mixtures of log-normal distributions, and the two features were also highly correlated. Therefore, we set the joint, state-dependent distribution of the observations to be a bivariate log-normal distribution.

Recall that we used thresholds of $m_{s,t} \geq 0.5$ and $d_{s,t} \geq 30$ to define biologically relevant dives. However, we modelled these observations using a two-dimensional log-normal distribution whose sample space is $\mathbb{R}_{>0}^2$, so our model is misspecified. We could use a truncated multivariate log-normal distribution instead, but many HMM software packages do not incorporate truncated log-normal distributions by default [23, 47], and several ecological studies make this modelling choice as well [19, 32, 43]. We therefore use a non-truncated log-normal distribution for simplicity and reproducibility.

Again, we modelled each killer whale dive profile as independent from the other dive profiles, but with shared parameters. Denote the observations from whale s as $\mathbf{y}_s = \{y_{s,t}\}_{t=1}^{T_s}$ and the labels from whale s as $\mathbf{z}_s = \{z_{s,t}\}_{t=1}^{T_s}$, where T_s is the number of dives associated with whale s . Then, the total

likelihood for the model with weight α and parameters $\boldsymbol{\delta}, \boldsymbol{\Gamma}, \boldsymbol{\theta}$ and $\boldsymbol{\beta}$ is $\prod_{s=1}^{11} \mathcal{L}_\alpha(\mathbf{y}_s, \mathbf{z}_s; \boldsymbol{\delta}, \boldsymbol{\Gamma}, \boldsymbol{\theta}, \boldsymbol{\beta})$, where \mathcal{L}_α is defined in Eq (11).

Model selection and evaluation

We fit five different candidate PHMMs corresponding to five different values of α . In line with the cross-validation procedure described earlier, we tested $\alpha = 0$, which ignores all unlabelled data; $\alpha = 1$, which gives equal weight to all observations; and $\alpha = |\mathcal{T}|/(T - |\mathcal{T}|) = 0.049$, which approximately balances the contribution of labelled and unlabelled observations. For completeness, we also tested $\alpha = 0.025$, which averages $\alpha = 0$ and $\alpha = 0.049$; and $\alpha = 0.525$, which averages $\alpha = 0.049$ and $\alpha = 1$.

We randomly divided each killer whale dive profile into two ‘‘sub-profiles’’ of contiguous dives such that both sub-profiles had an equal number of labels. The resulting 22 sub-profiles were used as folds in a cross-validation scheme to estimate the probability of each dive’s type conditioned on the observations (i.e., $\mathbb{P}(X_{s,t} = i \mid \mathbf{Y}_s = \mathbf{y}_s)$ for $s = 1, \dots, 11$; $t = 1, \dots, T_s$; and $i = 1, 2, 3$). We then calculated the sensitivity, specificity, and area under the receiver operating characteristic curve (AUC) associated with identifying each dive type. Sensitivity is the proportion of dives that were observed to be a certain type that were correctly identified as that type (i.e. the true positive rate). Specificity is the proportion of dives that were observed to not be of a certain type that were correctly identified as not that type (i.e. the true negative rate). AUC balances sensitivity and specificity and takes values between 0 and 1, where higher is better [4]. We also ran the Viterbi algorithm on each fold within the cross-validation procedure and plotted the resulting dive profiles as a visual model evaluation tool [48].

Results

The PHMMs with $\alpha \in (0, 1)$ tended to obtain better results for cross-validated sensitivity, specificity, and AUC, demonstrating the effectiveness of our weighted likelihood approach (Fig 3). Compared to the PHMMs with $\alpha = 0$ and $\alpha = 1$, the PHMM with $\alpha = 0.049$ had the best sensitivity for foraging dives and travelling dives, and it had the second-best sensitivity for resting dives. It had the best specificity for resting dives and travelling dives, and its specificity for foraging dives was comparable to the other models. In addition, the PHMM with $\alpha = 0.049$ had an AUC for resting that was comparable or better than the other PHMMs (0.866), but it had the best AUC for foraging (0.955) and the best AUC for travelling (0.926). Results for the PHMMs with $\alpha = 0.025$ and $\alpha = 0.525$ are similar to the PHMM with $\alpha = 0.049$ (see Appendix S1).

The PHMMs with $\alpha \in (0, 1)$ were also more biologically interpretable compared to those with $\alpha = 0$ and $\alpha = 1$. Namely, for the PHMMs with $\alpha \in (0, 1)$, the time series of decoded dive types contained long sequences of a single dive type (Fig 4). This behaviour matches prior studies that model killer whale behaviours as lasting from tens of minutes to hours [25]. In comparison, the PHMM with $\alpha = 1$ resulted in a dive profile that switched relatively frequently between foraging and resting dives (e.g., Fig 4a). The PHMM with $\alpha = 0$ produced better results than the PHMM with $\alpha = 1$, but it still estimated some rapidly switching dive types (e.g., Fig 4c).

The PHMM that completely ignored unlabelled dives ($\alpha = 0$) obtained better results than the PHMM that fully included the unlabelled dives ($\alpha = 1$). While one may expect that more data should improve accuracy, including unlabelled data is known to degrade the performance of a classifier in certain situations [39]. It is thus natural that the optimal approach for this case study neither fully included nor totally ignored the labelled dive types.

Finally, we used the PHMM with $\alpha = 0.049$ to estimate how often the northern and southern resident killer whales engaged in foraging behaviour. In particular, we fit the PHMM to the entire data set, including all labels, and then ran the forward-backward algorithm on all whales and dives to calculate $\mathbb{P}(X_{s,t} = 3 \mid \mathbf{Y}_s)$ for $t = 1, \dots, T_s$ and $s = 1, \dots, 11$. We then labelled dive t of whale s as foraging if its decoded probability of foraging was above 50%. Using this procedure, we estimated that southern resident killer whales foraged for 5.47 hours, or 32.0% of the time, and that northern residents foraged for 17.90 hours, or 26.8% of the time. This sample size was very small

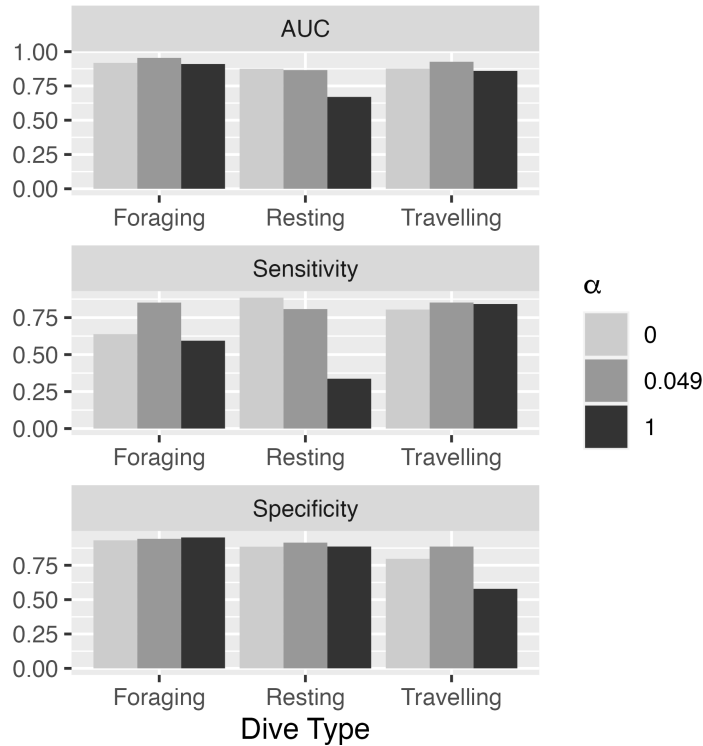
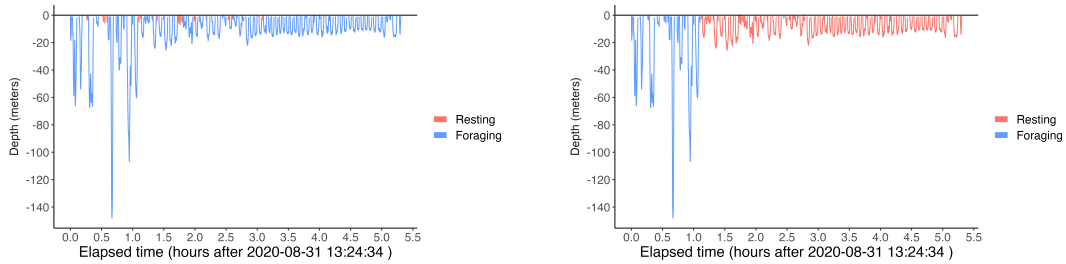
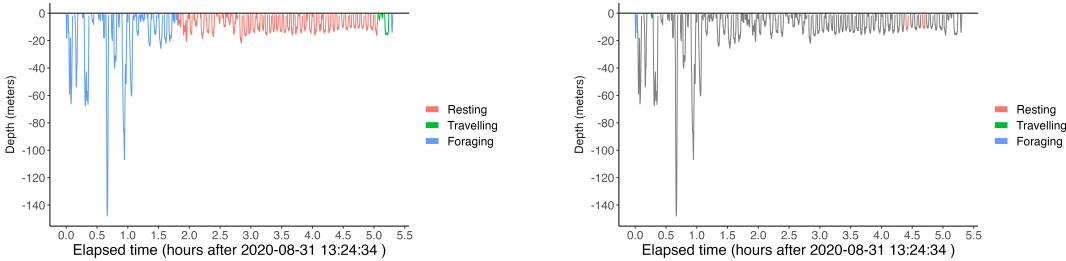


Fig 3. Sensitivity, specificity, and AUC values associated with each dive type. True values are determined via the drone-detected dive types. The PHMMs for each value of α were fit using the entire dataset with a selected sub-profile held out. Then, the dives for that sub-profile were estimated by using the forward-backward algorithm on the sub-profile with the drone-detected labels removed. We repeated this process for every sub-profile to get a full set of estimated dive types. Results for PHMMs with $\alpha = 0.025$ and $\alpha = 0.525$ are in Appendix S1.



(a) Decoded dives for PHMM with $\alpha = 1.000$ (the “natural” weighting). (b) Decoded dives for PHMM with $\alpha = 0.049$.



(c) Decoded dives for PHMM with $\alpha = 0.000$ (treating the unlabelled observations as missing). (d) Dive profile with true drone-detected labels.

Fig 4. Viterbi-decoded dives for a profile of killer whale D26 (Male, 10 years old) and several different PHMMs. Each PHMM was fit to the dataset with the sub-profile held out. Then the Viterbi algorithm was used on the held-out dataset with its labels removed in order to test the predictive performance of each PHMM.

(2 southern residents and 9 northern residents), and the sample of southern residents in particular was made up entirely of adult males killer whales, which are expected to forage more than other age-sex groups [45]. Nonetheless, our results are consistent with Tennessen et al. [45], who found that southern residents spent less time travelling and resting compared to northern resident killer whales.

Case study 2: identification of killer whale foraging

The second case study focused on identifying successful foraging events within the killer whale dives. Therefore, we divided all dives deeper than 30 meters into sequences of two-second windows and modelled each sequence with a PHMM. The hidden Markov chain was a sequence of unobserved two-second subdive states, and the observations were summary statistics calculated from each two-second window. We defined six possible subdive state behaviours: descent, bottom, prey chase, prey capture, ascent with a fish, and ascent without a fish.

Data processing

We defined a killer whale dive identically to the previous case study, but only included dives deeper than 30 meters because Wright et al. [50] found that killer whale prey captures usually occur below that depth. In addition, adult Chinook have also been found throughout the water column to depths exceeding 100 m, particularly in areas where the risk of predation appears high [36,37]. We divided each dive into two-second windows and calculated summary statistics that were identified by Tennessen et al. [44] to be indicative of foraging behaviour: change in depth ($d_{s,t}$ for dive s and window t), heading total variation ($h_{s,t}$), and jerk peak ($j_{s,t}$). Change in depth was defined as the last depth reading of the window minus the first depth reading of the window in meters. Heading total variation was determined by calculating the difference between heading readings every

1/50 of a second (in radians), taking the absolute value of that difference, and summing up all of the differences over the course of the two-second window. Jerk peak was calculated by taking the difference between acceleration vectors every 1/50 of a second (in meters per second squared), taking the magnitude of that difference, and then calculating the maximum over each two-second interval. To adjust for variation between dives and tags, we also divided the jerk peak of each two-second window by the median jerk peak for the bottom 70% of its corresponding dive [44]. In summary, the observation associated with whale s and window t was denoted as $y_{s,t} = (d_{s,t}, h_{s,t}, j_{s,t})$. This process resulted in a total of $S = 130$ dives and $T = 15821$ two-second windows.

To label windows associated with prey capture, we used a process inspired by previous work on killer whale foraging [44, 50]. First, crunching sounds associated with prey handling were identified from the hydrophone using the behavioural analysis software BORIS [9]. Crunching sounds associated with foraging were corroborated using video evidence of prey handling as well as audio observations of echolocation clicks. Next, Wright et al. [50] found that killer whales catch prey immediately before ascending, so we ignored crunches that occurred more than 30 seconds before a dive’s “ascent” phase as defined by Tennessen et al. [44]. Namely, the “ascent” phase began the moment after the killer whale achieved a depth at least 70% of its maximum dive depth. If the first non-ignored crunch occurred *before* “ascent”, we labelled its window as “prey capture”. If the first non-ignored crunch was heard *during* “ascent”, then the exact moment of prey capture was ambiguous, so we labelled the final window of the dive as “ascent with a fish”.

We were also able to obtain some window labels not associated with prey capture. First, if the video recorder was on for the entire dive, but there was no audible crunch or visual indication of foraging (e.g., scales), then we labelled the final window of the dive as “ascent without a fish”. Second, we labelled the first window of every dive as “descent”. Formally, the label associated with window t of dive s was denoted as $z_{s,t} \in \{\emptyset, 1, 2, 3, 4, 5, 6\}$, where each possible value of $z_{s,t}$ corresponds to no label ($z_{s,t} = \emptyset$), descent ($z_{s,t} = 1$), bottom ($z_{s,t} = 2$), chase ($z_{s,t} = 3$), capture ($z_{s,t} = 4$), ascent without a fish ($z_{s,t} = 5$), or ascent with a fish ($z_{s,t} = 6$). In total, we labelled 130 windows as “descent”, five windows as “capture”, two windows as “ascent with a fish”, and 19 windows as “ascent without a fish”. This resulted in $|\mathcal{T}| = 156$ labels, which make up less than 1% of the $T = 15821$ windows in total.

Model formulation

As mentioned before, we defined a PHMM with $N = 6$ subdive states: descent, bottom, chase, capture, ascent without a fish, and ascent with a fish. We assumed that all dives shared an initial distribution $\delta = (1 \ 0 \ 0 \ 0 \ 0 \ 0)$ and transition probability matrix Γ as shown in Eq (12).

$$\Gamma = \begin{pmatrix} \text{descent} & \text{bottom} & \text{chase} & \text{capture} & \text{ascent w/o fish} & \text{ascent w/ fish} & \\ \Gamma^{(1,1)} & \Gamma^{(1,2)} & 0 & 0 & \Gamma^{(1,5)} & 0 & \text{descent} \\ 0 & \Gamma^{(2,2)} & \Gamma^{(2,3)} & 0 & \Gamma^{(2,5)} & 0 & \text{bottom} \\ 0 & \Gamma^{(3,2)} & \Gamma^{(3,3)} & \Gamma^{(3,4)} & \Gamma^{(3,5)} & 0 & \text{chase} \\ 0 & 0 & 0 & \Gamma^{(4,4)} & 0 & \Gamma^{(4,6)} & \text{capture} \\ 0 & 0 & 0 & 0 & 1 & 0 & \text{asc w/o fish} \\ 0 & 0 & 0 & 0 & 0 & 1 & \text{asc w/ fish} \end{pmatrix} \quad (12)$$

For an intuitive visualization of how the Markov chain could evolve, see Fig 5. In short, this transition probability matrix reflects that marine mammal dives have distinct descent, bottom, and ascent phases [44], and that killer whales begin their ascent phase immediately after prey capture [50]. We also divided the bottom phase to include a low activity state (bottom) and a high activity state (chase), which is in line with results from Sidrow et al. [38].

Given that $X_{s,t} = i$, we modelled change in depth with a normal distribution, heading total variation with a gamma distribution, and normalized jerk peak with a gamma distribution. To enforce that the killer whale does not ascend or descend on average during the bottom of its dive,

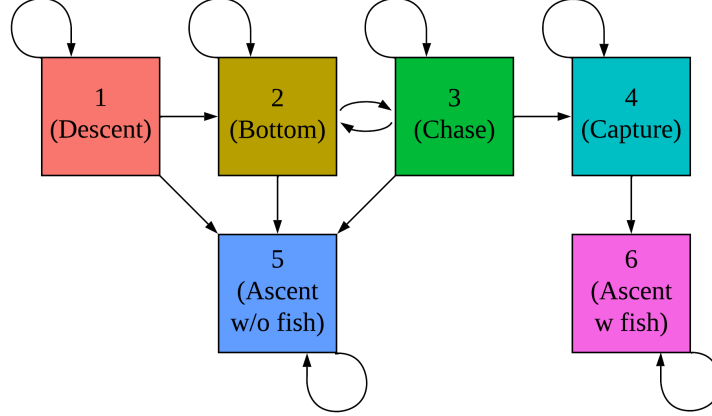


Fig 5. Visualization showing how the Markov chain \mathbf{X}_s can evolve within the second case study of killer whale foraging. Arrows correspond to non-zero entries in $\mathbf{\Gamma}$, where arrows point from row number to column number. Within a dive, a killer whale can proceed from descent, to bottom, to chase, to capture, to ascent with fish. It can also ascend without a fish at any time before capture, and it can switch between the bottom and chase states freely.

we set the state-dependent distributions of change in depth for the bottom, chase, and capture states to have a mean of zero. Further, we wanted to ensure that the model distinguished foraging based primarily on the “prey capture” subdive state rather than differences between the “ascent with a fish” and “ascent without a fish” states. As such, we set the two state-dependent distributions associated with ascent to be identical. Given the hidden state of a window $(X_{s,t})$, we also assumed that all summary statistics were independent. Denote the observations from dive s as $\mathbf{y}_s = \{y_{s,t}\}_{t=1}^{T_s}$ and the labels from dive s as $\mathbf{z}_s = \{z_{s,t}\}_{t=1}^{T_s}$. Then, we modelled all dives as independent, so the total likelihood for the model with weighting parameter α and parameters $\boldsymbol{\delta}, \mathbf{\Gamma}, \boldsymbol{\theta}$ and $\boldsymbol{\beta}$ was $\prod_{s=1}^{130} \mathcal{L}_\alpha(\mathbf{y}_s, \mathbf{z}_s; \boldsymbol{\delta}, \mathbf{\Gamma}, \boldsymbol{\theta}, \boldsymbol{\beta})$, where \mathcal{L}_α is defined in Eq (11).

Model evaluation

We fit five different PHMMs corresponding to $\alpha \in \{0.0001, 0.001, 0.01, 0.1, 1\}$. We did not include $\alpha = 0$ in this case study because we did not have labels associated with subdive states 2 and 3 (bottom and chase). Thus, if $\alpha = 0$, there were no observations that could be used to estimate the parameters of the state-dependent distribution parameters $\theta^{(2)}$ and $\theta^{(3)}$, and the model would not be identifiable.

In addition to the PHMMs, we also implemented the prey-capture identification method from Tennessen et al. [44] as a baseline. In particular, Tennessen et al. calculated three summary statistics for each dive: (1) the maximum of jerk during the bottom 70% of the dive, divided by the median jerk during the same period, (2) the absolute value of the killer whale’s roll at the moment of jerk peak, and (3) the circular variance of heading during the bottom 70% of the dive. Then, Tennessen et al. took the minimum value of every summary statistic over all confirmed prey capture dives to obtain thresholds for each of the three dive-level summary statistics. Finally, a dive was labelled as a successful foraging dive if *every* dive-level summary statistic surpassed that threshold.

We evaluated each model based on how well it predicted successful foraging dives. Note that the probability that dive s is a successful foraging dive is equal to the probability that it ends in either the “capture” or “ascent with a fish” state. In other words, it is the probability that window T_s of dive s has subdive state 4 (capture) or subdive state 6 (ascent with a fish), i.e. $\mathbb{P}(X_{s,T_s} \in \{4, 6\} \mid \mathbf{Y}_s = \mathbf{y}_s)$. To estimate this value, we randomly and equally split the seven labelled successful foraging dives and 19 labelled dives without successful foraging into four folds

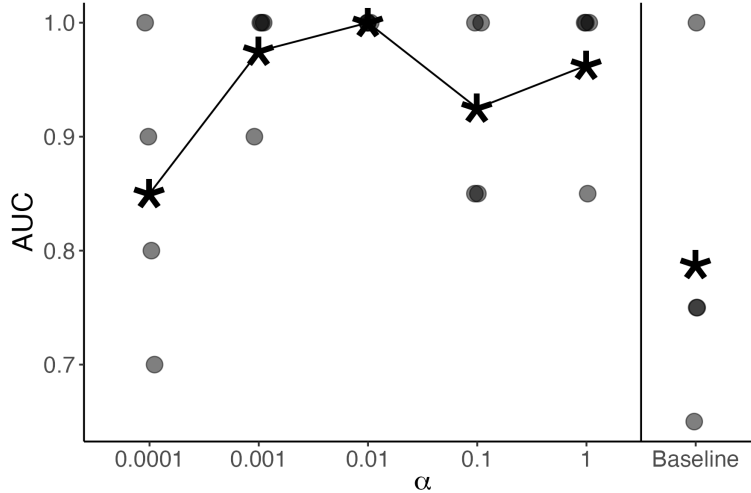


Fig 6. Four-fold, cross-validated area under the ROC curve (AUC) values for five PHMMs as well as the baseline method of Tennessen et al. [44]. Horizontal jitters have been added because dots occasionally fall on top of one another. Averages are shown as stars and connected with a line for the PHMM approaches.

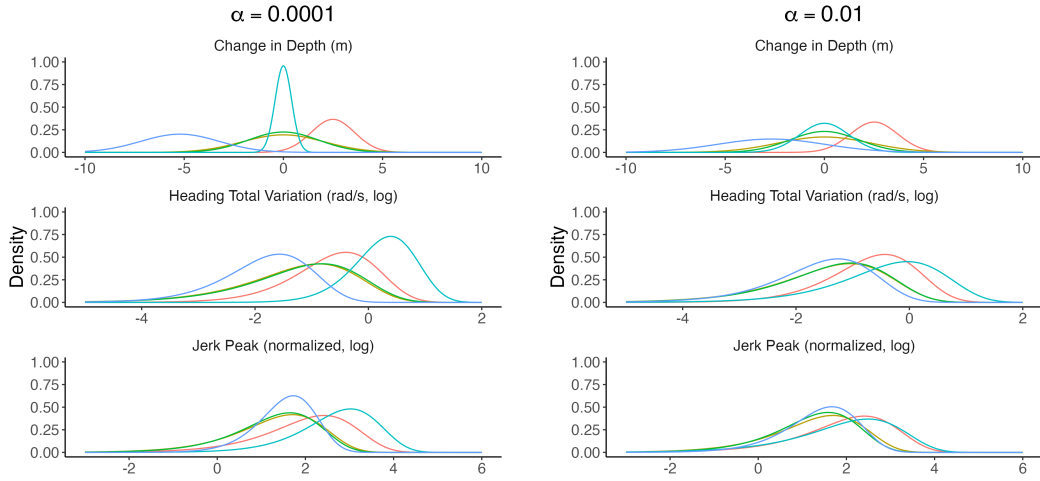
and performed cross validation with the forward-backward algorithm. We calculated AUC values within each fold and reported their averages (see Fig 6). Finally, we also fit each PHMM to the entire dataset to visualize their state-dependent distributions (see Fig 7).

Results

Our method outperformed the baseline of Tennessen et al. [44], which had an average AUC of 0.79. In comparison, the PHMM with $\alpha = 0.0001$ had an average AUC of 0.90, the PHMM with $\alpha = 1.0$ had an AUC of 0.96, and the PHMM with $\alpha = 0.01$ had a perfect AUC of 1 across all four folds (Fig 6). Thus, not only did using a PHMM produce better predictive performance over existing baselines, but using $\alpha \in (0, 1)$ (namely $\alpha = 0.01$ here) improved predictive performance over $\alpha = 0$ and $\alpha = 1$.

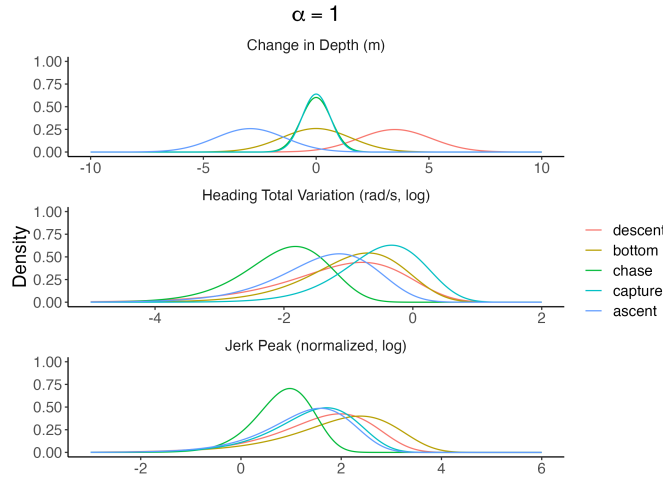
The biological interpretation of each PHMM heavily depended on the weight α . For example, the “bottom” and “chase” states looked very similar for the PHMMs with $\alpha \leq 0.01$, but the two states were better separated within the PHMM with $\alpha = 1$ (Fig 7). However, the “bottom” subdivide state had higher mean jerk peak and heading total variation than the “chase” subdivide state for the PHMM with $\alpha = 1$. These results are the opposite of what ecologists expect biologically, indicating that a large separation between state-dependent distributions is not always more biologically interpretable. We conjecture that the “bottom” and “chase” subdivide states are particularly unintuitive partially because there are no labels associated with either of these subdivide states (i.e. $z_{s,t} \neq 2, 3$ for any s or t). As a result, there is little information for the model to differentiate the two subdivide states.

Differences between each model’s distribution for the capture state appeared to impact predictive performance. For example, the PHMM with $\alpha = 0.0001$ estimated a relatively high mean and low standard deviation for heading total variation (middle panel of Fig 7a). As such, it failed to identify a prey capture event in which heading total variance was highly variable (Fig 8). Alternatively, the PHMM with $\alpha = 1$ estimated a relatively low mean for heading variation (middle panel of Fig 7c). As a result, it was often too sensitive and decoded some dives that lacked successful foraging as containing a prey capture state (Fig 9). The PHMM with $\alpha = 0.01$ estimated a high mean and a high standard deviation for heading total variation (middle panel of Fig 7b). It correctly identified a wide variety of labelled foraging dives, but it was not overly sensitive and correctly identified low-activity dives as lacking successful foraging.



(a) $\alpha = 0.0001$

(b) $\alpha = 0.01$



(c) $\alpha = 1$

Fig 7. State-dependent densities for change in depth (top panels), heading total variation (middle panels), and normalized jerk peak (bottom panels) for PHMMs with $\alpha = 0.0001$ (top left), $\alpha = 0.01$ (top right), and $\alpha = 1$ (bottom). Densities are coloured according to their corresponding subdive state. Parameters were estimated using the entire killer whale dataset (i.e. no cross-validation was performed). For a given observation $Y_{s,t}$, all features were assumed to be independent after conditioning on the subdive state $X_{s,t}$. Note that the “ascent with a fish” and “ascent without a fish” states were assumed to have identical distributions, so both are listed simply as “ascent”.

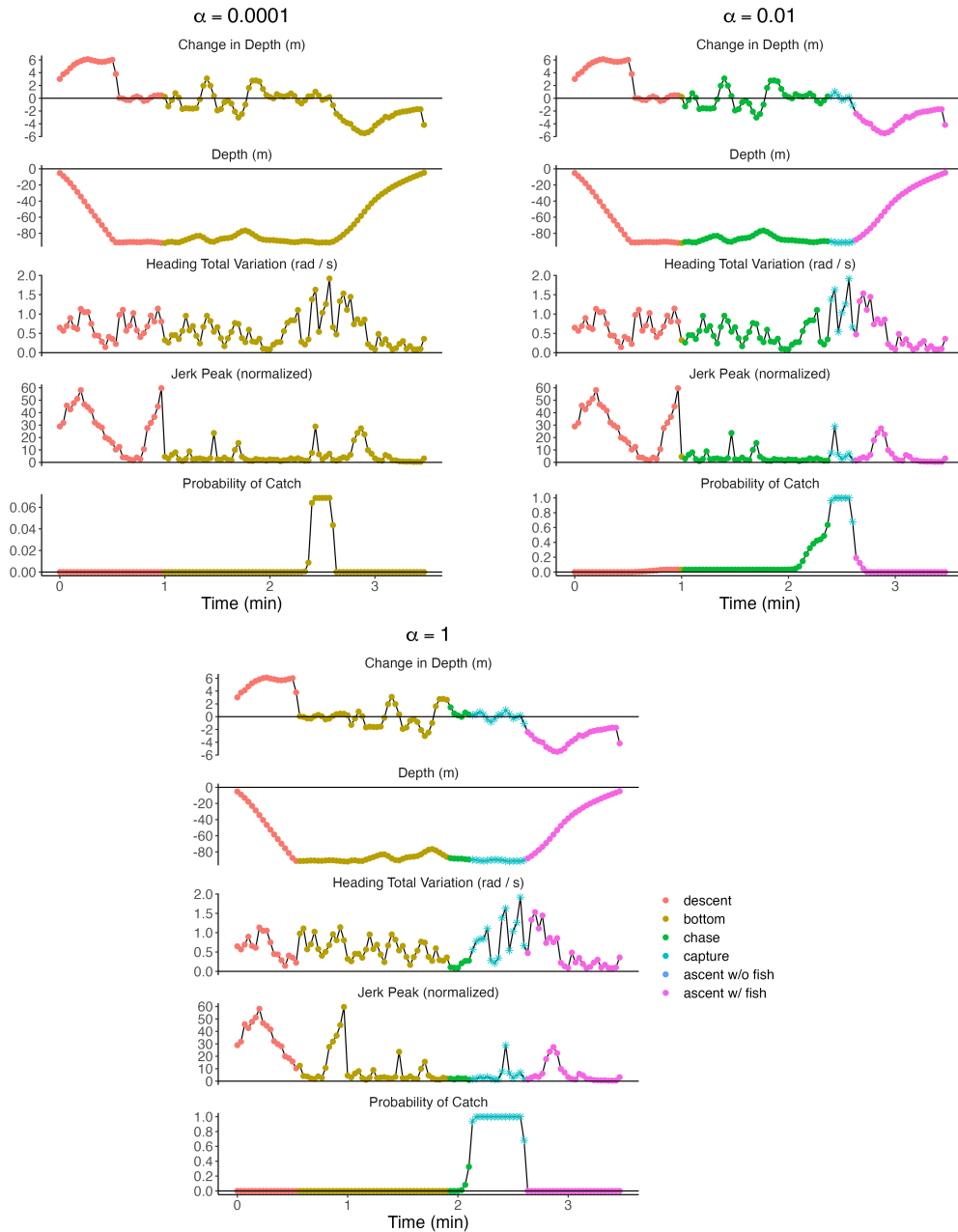


Fig 8. Dive profiles, observations, and the decoded probability that each window is the “capture” state for a selected successful foraging dive in case study 2. PHMMs with $\alpha = 0.0001$ (top left), $\alpha = 0.01$ (top right) and $\alpha = 1$ (bottom) are shown. Each subplot displays change in depth (top panel), raw depth (second panel), heading total variation (third panel), normalized jerk peak (fourth panel), and probability of “capture” (bottom panel). Observations are coloured according to the most-likely sequence of hidden states as determined by the Viterbi algorithm. The estimated probability of successful foraging, $\mathbb{P}(X_{s,T_s} \in \{4, 6\} \mid \mathbf{Y}_s = \mathbf{y}_s)$, is 0.069 for $\alpha = 0.0001$, 1 for $\alpha = 0.01$, and 1 for $\alpha = 1$.

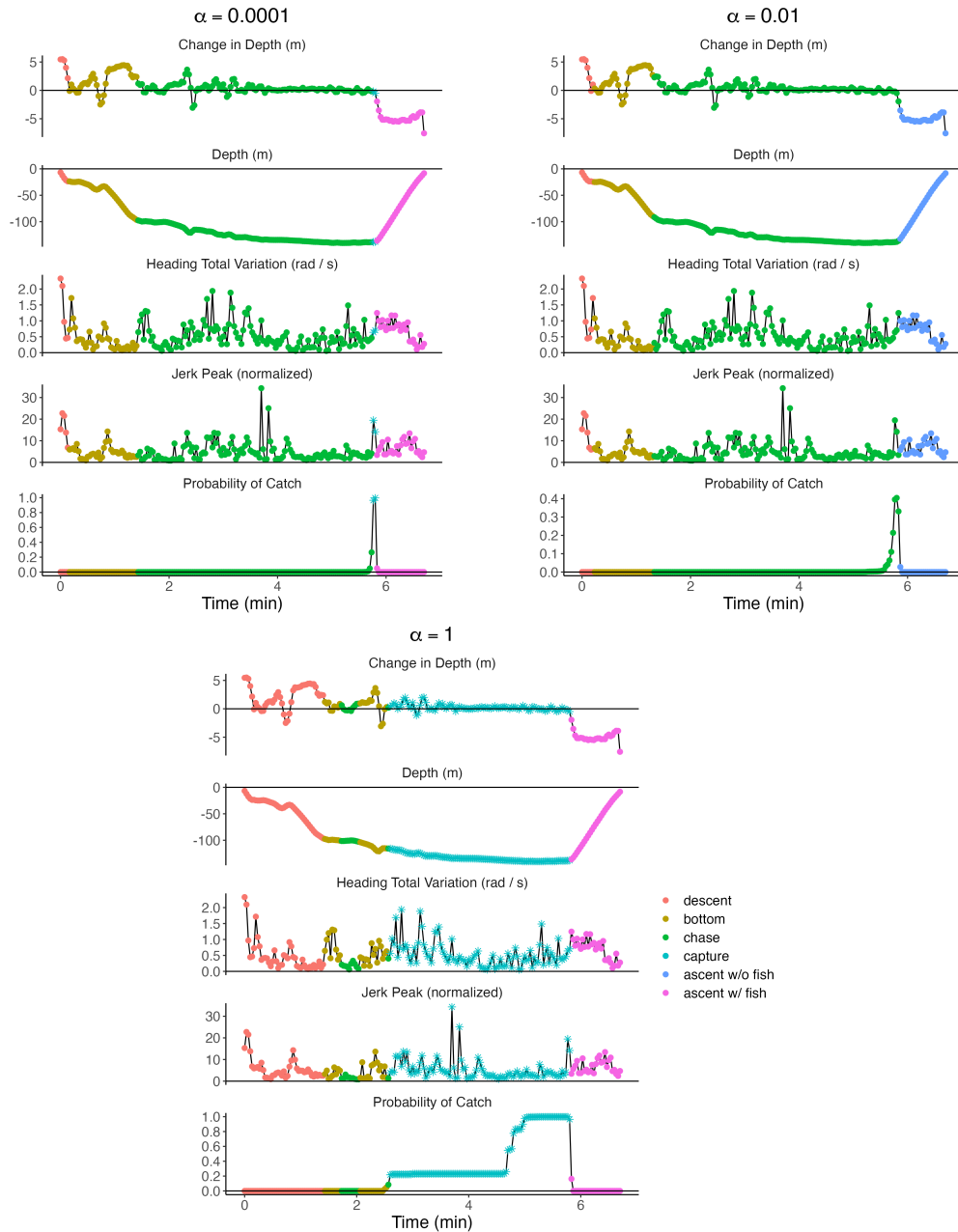


Fig 9. Dive profiles, observations, and the decoded probability that each window is the "capture" state for a selected dive with no foraging in case study 2. PHMMs with $\alpha = 0.0001$ (top left), $\alpha = 0.01$ (top right) and $\alpha = 1$ (bottom) are shown. Each subplot displays change in depth (top panel), raw depth (second panel), heading total variation (third panel), normalized jerk peak (fourth panel), and probability of "capture" (bottom panel). Observations are coloured according to the most-likely sequence of hidden states as determined by the Viterbi algorithm. The estimated probability of successful foraging, $\mathbb{P}(X_{s,T_s} \in \{4, 6\} \mid \mathbf{Y}_s = \mathbf{y}_s)$, is 1 for $\alpha = 0.0001$, 0.414 for $\alpha = 0.01$, and 1 for $\alpha = 1$.

Finally, we used the PHMM with $\alpha = 0.01$ to estimate the total number of successful foraging dives from southern and northern resident killer whales in this data set. In particular, we fit the full model to the entire dataset, including labels, and then ran the forward-backward algorithm on all unlabelled dives to estimate the probability that each unlabelled dive was a successful foraging dive, $\mathbb{P}(X_{s,T_s} \in \{4, 6\} \mid \mathbf{Y}_s = \mathbf{y}_s)$ for $s = 1, \dots, 130$. Then, we labelled dive s as a successful foraging dive if the estimate of this probability was above 50%. This process resulted in 6 estimated successful foraging dives from southern resident killer whales and 37 estimated successful foraging dives from northern resident killer whales. After combining these results with those from the first case study, we found that southern resident killer whales caught an average of 1.03 fish per hour of foraging effort, while northern resident killer whales caught an average of 2.00 fish per hour of foraging effort. These results support the finding that northern resident killer whales have more foraging success compared to southern residents [45]. However, our sample size is small (2 southern resident killer whales and 9 northern resident killer whales), and the tag attachments were relatively short and thus provided only a snapshot in time. For example, some killer whales were tagged right after foraging, so a tag attachment of several hours recorded no foraging events. Future studies can use the methods outlined here with larger sample sizes and longer tag attachments to further investigate the differences between northern and resident killer whale foraging success.

5 Discussion

In this work, we incorporated sparse labels into an HMM in a natural way that changes the influence of unlabelled observations and demonstrably improves predictive performance. In particular, we weighted observations without associated labels within the likelihood of the HMM using a parameter $\alpha \in [0, 1]$. On the extremes, $\alpha = 0$ corresponds to an HMM which totally ignores unlabelled data and $\alpha = 1$ corresponds to a traditional, unweighted HMM. Cross-validated accuracy metrics can be used to find an optimal value of α between these extremes.

We used this weighted likelihood approach to effectively leverage underwater video and audio data and generate a more detailed description of killer whale foraging behaviour. In addition to better performance, our method has two additional benefits compared to previous methods. First, it estimates the probability that each dive is a successful foraging dive instead of outputting a binary label. This allows practitioners to set a threshold to balance the false positive and false negative rates. Second, our method also categorizes subdive states so practitioners can simultaneously categorize the subdive behaviour of the killer whale while they estimate successful foraging dives.

Future work can quantify exactly how the density of labels and level of model misspecification affect the value of α that optimizes prediction accuracy and model fit. The biological interpretability and predictive accuracy of the model from the first case study were optimized for $\alpha \approx 0.05$. In the second case study, the model had better predictive performance for $\alpha = 0.01$, and each PHMM had distinct biological interpretations for $\alpha \leq 0.01$ and $\alpha > 0.01$. The “bottom” and “chase” subdive states were better separated for the PHMMs with $\alpha > 0.01$, but not necessarily in a way that was biologically natural. It is intuitive that subdive states with no labels were better separated within PHMMs that weighted unlabelled observations more heavily. Quantifying the precise relationship between α and the state-dependent distributions is a promising direction for future research.

As is common in movement ecology, our case studies had a small number of labels, which can negatively impact the reliability of cross-validation. Therefore, future work can apply this weighted likelihood approach to case studies with more labels, potentially from other fields. We also performed case studies in which we were confident in our labels. Future work can focus on how including labels affects the performance of the PHMM when researchers are less confident in their labels and infer β as a parameter of the PHMM.

Although we did not have a large enough sample size or long enough tag deployments to draw definitive conclusions, the findings from our method are in line with those from Tennessen et al. [45], who conducted a comprehensive study of foraging behaviour in northern and southern resident killer whales. In particular, our results support their findings that northern resident killer whales tend

to spend more time travelling and resting compared to southern residents, and that the northern residents tend to catch more fish per unit of effort compared to the southern residents.

Our weighted likelihood approach improves the estimates of unobserved labels from a time series, but it cannot ensure the interpretability and reliability of the labels themselves. For example, recent studies have found adult Chinook salmon migrating in the upper 30 meters of the water column in addition to the deep depths that we explored in this paper [10]. This suggests that killer whales likely employ two foraging strategies to exploit the dichotomy of Chinook swimming tactics. The first strategy that we and others have documented [45,49] involves repeatedly diving to depths exceeding 30 m to locate and pursue Chinook in areas where salmon are holding or evading predators. The other may involve killer whales repeatedly searching medium water depths (10–30 m) while travelling using echolocation to identify and capture salmon near the surface or by pursuing them to depth. As such, the foraging labels from the first case study likely correspond only to deep foraging dives associated with this first foraging strategy. While we are confident that the PHMM accurately identified resting and foraging dives, we recognize that the killer whales were also likely searching for Chinook during “travelling” dives. In fact, we occasionally found echolocation clicks that coincided with dives labelled as travelling in our case study. It may thus be possible to further refine and validate the PHMM using echolocation data recorded by the tags to better categorize the behavioural states of killer whale travelling dives based on their depths and durations relative to the recent information on adult Chinook migratory behaviour.

We primarily focused on identifying the behaviour of killer whales, but incorporating sparse labels into complex HMMs is a common modelling problem across a variety of use cases and disciplines. In addition, complicated time series data are increasingly common as sensing technology continues to improve [30]. As such, the modelling approach developed here can help researchers effectively model complicated, sparsely labelled time series to optimize prediction accuracy and model fit.

Acknowledgments

The killer whale data were collected under University of British Columbia Animal Care Permit number A19-0053 and Fisheries and Oceans Canada Marine Mammal Scientific License for Whale Research number XMMS 6 2019. We thank Mike deRoos and Chris Hall for assistance in the field with tag deployments, Taryn Scarff for assistance with drone deployments, the M/V Gikumi captain and crew, and Keith Holmes for piloting the drone, filming the killer whales, and assisting in synchronizing time stamps. Drone footage was collected in partnership with Hakai Institute. This research was enabled in part by support provided by WestGrid (www.westgrid.ca) and Compute Canada (www.computecanada.ca). We acknowledge the support of the Natural Sciences and Engineering Research Council of Canada (NSERC) as well as the support of Fisheries and Oceans Canada (DFO). We thank the University of British Columbia and the Four-Year Doctoral Fellowship program. We acknowledge the Canadian Statistical Sciences Institute (CANSSI) for its support. We appreciate the support of the Canada Research Chairs program. We acknowledge support from the BC Knowledge Development Fund. We thank Canada Foundation for Innovation for its support.

References

- [1] T. Adam, C. Griffiths, V. Leos Barajas, E. Meese, C. Lowe, P. Blackwell, D. Righton, and R. Langrock. Joint modelling of multi-scale animal movement data using hierarchical hidden Markov models. *Methods in Ecology and Evolution*, 10(9):1536–1550, 06 2019.
- [2] A. N. Allen, J. A. Goldbogen, A. S. Friedlaender, and J. Calambokidis. Development of an automated method of detecting stereotyped feeding events in multisensor data from tagged orqual whales. *Ecology and Evolution*, 6(20):7522–7535, 2016.

- [3] P. G. Bagos, T. D. Liakopoulos, and S. J. Hamodrakas. Maximum likelihood and conditional maximum likelihood learning algorithms for hidden Markov models with labeled data: application to transmembrane protein topology prediction. In *Proceedings of the International Conference on Computational Methods in Sciences and Engineering, ICCMSE '03*, page 47–55. World Scientific Publishing Co., Inc., 2003.
- [4] A. P. Bradley. The use of the area under the roc curve in the evaluation of machine learning algorithms. *Pattern Recognition*, 30(7):1145–1159, 1997.
- [5] D. E. Cade, W. T. Gough, M. F. Czapanskiy, J. A. Fahlbusch, S. R. Kahane-Rapport, J. M. J. Linsky, et al. Tools for integrating inertial sensor data with video bio-loggers, including estimation of animal orientation, motion, and position. *Animal Biotelemetry*, 9, 2021.
- [6] G. Carroll, D. Slip, I. Jonsen, and R. Harcourt. Supervised accelerometry analysis can identify prey capture by penguins at sea. *Journal of Experimental Biology*, 217:4295–4302, 2014.
- [7] O. Chapelle, B. Schölkopf, and A. Zien, editors. *Semi-supervised learning*. The MIT Press, 2006.
- [8] Fisheries and Oceans Canada. Amended recovery strategy for the northern and southern resident killer whales (orcinus orca) in canada. Species at Risk Act Recovery Strategy Series, 2018.
- [9] O. Friard and M. Gamba. Boris: a free, versatile open-source event-logging software for video/audio coding and live observations. *Methods in Ecology and Evolution*, 7(11):1325–1330, 2016.
- [10] B. J. L. Hendriks. Behaviour and movement of return migrating adult chinook salmon (oncorhynchus tshawytscha) through the salish sea, 2024.
- [11] N. J. Higham and L. Lin. A schur–padé algorithm for fractional powers of a matrix. *SIAM Journal on Matrix Analysis and Applications*, 32(3):1056–1078, 2011.
- [12] F. Hu. The asymptotic properties of the maximum-relevance weighted likelihood estimators. *The Canadian Journal of Statistics*, 25(1):45–59, 1997.
- [13] F. Hu, W. F. Rosenberger, and J. V. Zidek. Relevance weighted likelihood for dependent data. *Metrika*, 51(3):223–243, Sep 2000.
- [14] F. Hu and J. V. Zidek. The weighted likelihood. *Canadian Journal of Statistics*, 30(3):347–371, 2002.
- [15] S. Ji, L. T. Watson, and L. Carin. Semisupervised learning of hidden markov models via a homotopy method. *IEEE Transactions on Pattern Analysis and Machine Intelligence*, 31(2):275–287, 2009.
- [16] R. Joy, D. Tollit, J. Wood, A. MacGillivray, Z. Li, K. Trounce, and O. Robinson. Potential benefits of vessel slowdowns on endangered southern resident killer whales. *Frontiers in Marine Science*, 6, 2019.
- [17] N. J. Klappstein, L. Thomas, and T. Michelot. Flexible hidden markov models for behaviour-dependent habitat selection. *Movement Ecology*, 11(1):30, Jun 2023.
- [18] A. Krogh. Two methods for improving performance of a HMM and their application for gene finding. *Proceedings. International Conference on Intelligent Systems for Molecular Biology*, 5:179–86, 1997.

- [19] V. Leos-Barajas, E. J. Gangloff, T. Adam, R. Langrock, F. M. van Beest, J. Nabe-Nielsen, and J. M. Morales. Multi-scale modeling of animal movement and general behavior data using hidden Markov models with hierarchical structures. *Journal of Agricultural, Biological and Environmental Statistics*, 22(3):232–248, 02 2017.
- [20] D. Lusseau, D. Bain, R. Williams, and J. Smith. Vessel traffic disrupts the foraging behavior of southern resident killer whales *orcinus orca*. *Endangered Species Research*, 6(3):211–221, 2009.
- [21] B. T. McClintock, R. King, L. Thomas, J. Matthiopoulos, B. J. McConnell, and J. M. Morales. A general discrete-time modeling framework for animal movement using multistate random walks. *Ecological Monographs*, 82(3):335–349, 2012.
- [22] B. T. McClintock, R. Langrock, O. Gimenez, E. Cam, D. L. Borchers, R. Glennie, and T. A. Patterson. Uncovering ecological state dynamics with hidden Markov models. *Ecology Letters*, 23(12):1878–1903, 10 2020.
- [23] B. T. McClintock and T. Michélot. momentuHMM: R package for generalized hidden Markov models of animal movement. *Methods in Ecology and Evolution*, 9(6):1518–1530, 2018.
- [24] J. McInnes, K. Lester, L. Dill, C. Mathieson, P. West-Stap, S. Marcos, and A. Trites. Foraging behaviour and ecology of transient killer whales within a deep submarine canyon system. *PLOS ONE*, 19(03), 03 2024.
- [25] T. M. McRae, B. L. Volpov, E. Sidrow, S. M. E. Fortune, M. Auger-Méthé, N. Heckman, and A. W. Trites. Killer whale respiration rates. *PLOS ONE*, 19(5):1–26, 05 2024.
- [26] C. C. Murray, L. C. Hannah, T. Doniol-Valcroze, B. M. Wright, E. H. Stredulinsky, J. C. Nelson, A. Locke, and R. C. Lacy. A cumulative effects model for population trajectories of resident killer whales in the northeast pacific. *Biological Conservation*, 257:109124, 2021.
- [27] K. Nigam, A. K. McCallum, S. Thrun, and T. Mitchell. Text classification from labeled and unlabeled documents using em. *Machine Learning*, 39:103–134, 05 2000.
- [28] D. P. Noren. Estimated field metabolic rates and prey requirements of resident killer whales. *Marine Mammal Science*, 27(1):60 – 77, 01 2011.
- [29] M. B. Ogburn, A.-L. Harrison, F. G. Whoriskey, S. J. Cooke, J. E. Mills Flemming, and L. G. Torres. Addressing challenges in the application of animal movement ecology to aquatic conservation and management. *Frontiers in Marine Science*, 4, 2017.
- [30] T. A. Patterson, A. Parton, R. Langrock, P. G. Blackwell, L. Thomas, and R. King. Statistical modelling of individual animal movement: an overview of key methods and a discussion of practical challenges. *Advances in Statistical Analysis*, 101:399–438, 07 2017.
- [31] E. Pirotta, E. W. J. Edwards, L. New, and P. M. Thompson. Central place foragers and moving stimuli: A hidden-state model to discriminate the processes affecting movement. *Journal of Animal Ecology*, 87(4):1116–1125, 2018.
- [32] N. J. Quick, S. Isojunno, D. Sadykova, M. Bowers, D. P. Nowacek, and A. J. Read. Hidden markov models reveal complexity in the diving behaviour of short-finned pilot whales. *Scientific Reports*, 7(1):45765, Mar 2017.
- [33] R Core Team. *R: A language and environment for statistical computing*. R Foundation for Statistical Computing, Vienna, Austria, 2023.
- [34] Z. Ren, R. Yeh, and A. Schwing. Not all unlabeled data are equal: learning to weight data in semi-supervised learning. In H. Larochelle, M. Ranzato, R. Hadsell, M. F. Balcan, and H. Lin, editors, *Advances in Neural Information Processing Systems*, volume 33, pages 21786–21797. Curran Associates, Inc., 2020.

- [35] S. Saldanha, S. L. Cox, T. Militão, and J. González-Solís. Animal behaviour on the move: the use of auxiliary information and semi-supervision to improve behavioural inferences from hidden markov models applied to gps tracking datasets. *Movement Ecology*, 11:41, 2023.
- [36] M. Sato, A. W. Trites, and S. Gauthier. Southern resident killer whales encounter higher prey densities than northern resident killer whales during summer. *Canadian Journal of Fisheries and Aquatic Sciences*, 78(11):1732–1743, 2021.
- [37] B. Saygili and A. Trites. Prevalence of chinook salmon is higher for southern than for northern resident killer whales in summer hot-spot feeding areas. *PLOS ONE*, in press, 2024.
- [38] E. Sidrow, N. Heckman, S. M. E. Fortune, A. W. Trites, I. Murphy, and M. Auger-Méthé. Modelling multi-scale, state-switching functional data with hidden Markov models. *Canadian Journal of Statistics*, 2021.
- [39] A. Singh, R. Nowak, and J. Zhu. Unlabeled data: now it helps, now it doesn't. In D. Koller, D. Schuurmans, Y. Bengio, and L. Bottou, editors, *Advances in Neural Information Processing Systems*, volume 21, pages 1–8. Curran Associates, Inc., 2008.
- [40] D. W. Stephens, J. S. Brown, and R. C. Ydenberg. *Foraging: behavior and ecology*. University of Chicago Press, 2008.
- [41] W. J. Sutherland. The importance of behavioural studies in conservation biology. *Animal Behaviour*, 56(4):801–809, 11 1998.
- [42] I. A. Tamposis, K. D. Tsirigos, M. C. Theodoropoulou, P. I. Kontou, and P. G. Bagos. Semi-supervised learning of hidden Markov models for biological sequence analysis. *Bioinformatics*, 35(13):2208–2215, 11 2018.
- [43] J. Tennessen, M. M. Holt, E. J. Ward, M. B. Hanson, C. K. Emmons, D. A. Giles, and J. T. Hogan. Hidden Markov models reveal temporal patterns and sex differences in killer whale behavior. *Scientific Reports*, 9:14951, 10 2019.
- [44] J. B. Tennessen, M. M. Holt, M. B. Hanson, C. K. Emmons, D. A. Giles, and J. T. Hogan. Kinematic signatures of prey capture from archival tags reveal sex differences in killer whale foraging activity. *Journal of Experimental Biology*, 222(3), 2019.
- [45] J. B. Tennessen, M. M. Holt, B. M. Wright, M. B. Hanson, C. K. Emmons, D. A. Giles, J. T. Hogan, S. J. Thornton, and V. B. Deecke. Divergent foraging strategies between populations of sympatric matrilineal killer whales. *Behavioral Ecology*, 34(3):373–386, 03 2023.
- [46] J. E. van Englan and H. H. Hoos. A survey on semi-supervised learning. *Machine Learning*, 109:373–440, 2020.
- [47] I. Visser and M. Speekenbrink. depmixs4: an r package for hidden markov models. *Journal of Statistical Software*, 36(7):1–21, 2010.
- [48] A. Viterbi. Error bounds for convolutional codes and an asymptotically optimum decoding algorithm. *IEEE Transactions on Information Theory*, pages 260–269, April 1967.
- [49] B. M. Wright, V. B. Deecke, G. M. Ellis, A. W. Trites, and J. K. B. Ford. Behavioral context of echolocation and prey-handling sounds produced by killer whales (*orcinus orca*) during pursuit and capture of pacific salmon (*oncorhynchus* spp.). *Marine Mammal Science*, 37(4):1428–1453, 2021.
- [50] B. M. Wright, J. K. B. Ford, G. M. Ellis, V. B. Deecke, A. D. Shapiro, B. C. Battaile, and A. W. Trites. Fine-scale foraging movements by fish-eating killer whales (*Orcinus orca*) relate to the vertical distributions and escape responses of salmonid prey (*Oncorhynchus* spp.). *Movement Ecology*, 5:3, 12 2017.

- [51] A.-K. Ylitalo, J. Heikkinen, and I. Kojola. Analysis of central place foraging behaviour of wolves using hidden markov models. *Ethology*, 127(2):145–157, 2021.
- [52] W. Zucchini, I. L. Macdonald, and R. Langrock. *Hidden Markov models for time series - an introduction using R*. CRC Press, 06 2016.

A Additional results from case study 1

This appendix recreates Figures 3 and 4 from the first case study for $\alpha = 0, 0.025, 0.049, 0.525, 1$. The results for $\alpha = 0.025$ and $\alpha = 0.525$ are very similar to those for $\alpha = 0.049$, but we include them here for completeness.

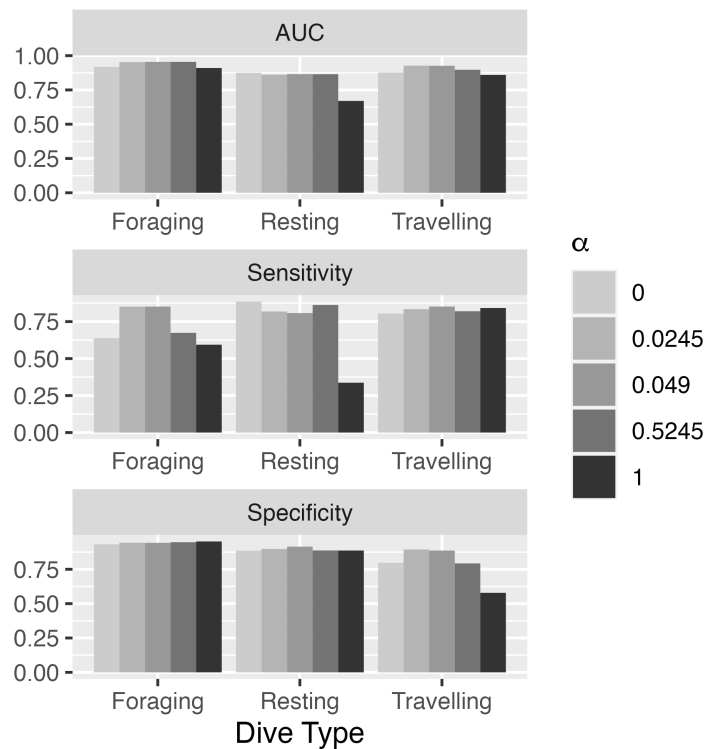
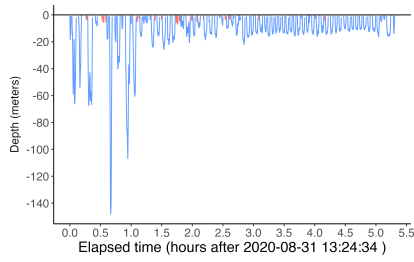
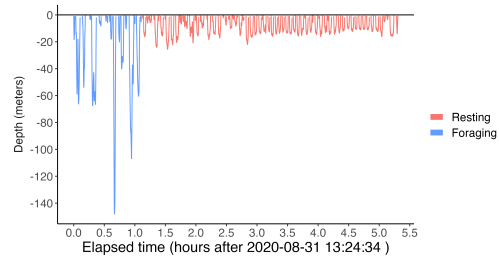


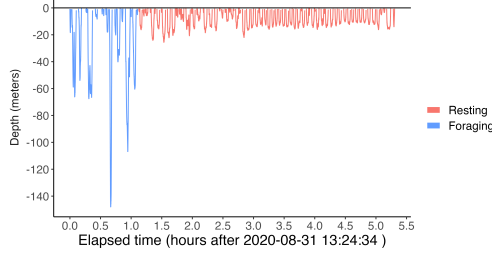
Fig 10. Sensitivity, specificity, and AUC values associated with each dive type. True values are determined via the drone-detected dive types. The PHMMs for each value of α were fit using the entire dataset with a selected sub-profile held out. Then, the dives for that sub-profile were estimated by using the forward-backward algorithm on the sub-profile with the drone-detected labels removed. We repeated this process for every sub-profile to get a full set of estimated dive types.



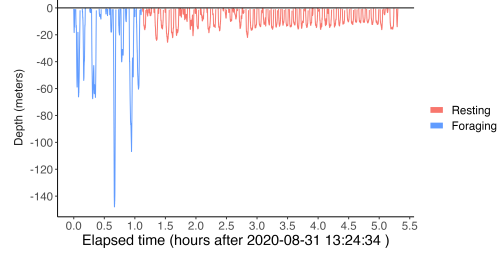
(a) Decoded dives for PHMM with $\alpha = 1.000$ (the “natural” weighting).



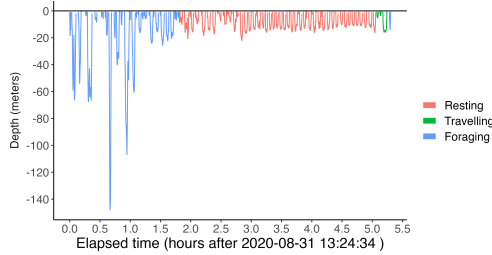
(b) Decoded dives for PHMM with $\alpha = 0.525$.



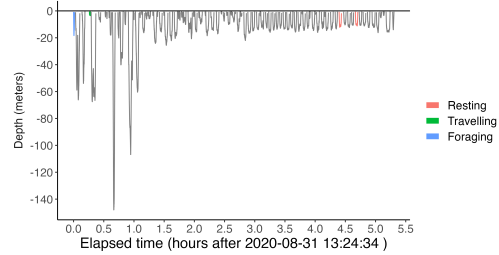
(c) Decoded dives for PHMM with $\alpha = 0.049$.



(d) Decoded dives for PHMM with $\alpha = 0.025$.



(e) Decoded dives for PHMM with $\alpha = 0.000$ (treating the unlabelled observations as missing).



(f) Dive profile with true drone-detected labels.

Fig 11. Viterbi-decoded dives for a given sub-profile and several different PHMMs. Each PHMM was fit to the dataset with the sub-profile held out. Then the Viterbi algorithm was used on the held-out dataset with its labels removed in order to test the predictive performance of each PHMM.